TEXTURE OF EQUAL CHANNEL ANGULAR PRESSED Cu INVESTIGATED BY ELECTRON BACK SCATTER DIFFRACTION AND X-RAY DIFFRACTION

ERHARD SCHAFLER[1,2]*, IRENEUSZ KOPACZ[2], REINHARD PIPPAN[2,3], HEIN-PETER STUEWE[2]

[1] *Institute of Materials Physics, University of Vienna, Strudlhofgasse 4, 1090 Vienna, Austria*
[2] *Erich Schmid Institute of Materials Science, Austrian Academy of Sciences, Jahnstrasse 12, A-8700 Leoben, Austria*
[3] *Christian Doppler Laboratory of Local Analysis of Deformation and Fracture, Jahnstrasse 12, A-8700 Leoben, Austria*

Received 15 July 2005, accepted 19 October 2005

The texture evolution of copper during route A and C – ECAP has been measured by standard X-ray technique as well as determined by electron back scatter diffraction, the latter monitors also the grain shape changes and the fragmentation during the high strain deformation. The orientation distribution functions were compared and discussed with respect to the subgrain division. With each pass of route A a further elongation and rotation of the grains is observable, while the alternating shear direction when processing route C results in roughly equi-axed grains. The high imposed strains cause formation of new boundaries subdividing the old grains. With proceeding deformation the increasing misorientation in this subgrain structure leads to further fragmentation of the material, what accounts for the good correspondence between microtexture determined by EBSD on relatively small areas and macrotexture obtained by XRD.

K e y w o r d s: severe plastic deformation, macrotexture, microtexture

1. Introduction

The production and characterization of submicro- and nanocrystalline materials has become a very important field in material science. Besides a series of extra-ordinary properties (enhanced soft magnetic properties, lowered thermal and electrical conductivity, enhanced diffusion coefficient) such materials exhibit both

*corresponding author, e-mail: erhard.schafler@univie.ac.at

high strength (because of small grain size) as well as extended ductility. Up to now, these materials could be only produced in small sample shapes (at most thin foils) by different methods (inert gas condensation, ball-milling and electrodeposition), which restricted their use to a few special applications. Since these materials can be achieved in bulk shape by special methods of severe plastic deformation their application to commercial areas could be extended.

A very important structural property for materials supplied to metal forming processes is the texture. There are several publications reporting the texture of ECAP-deformed materials: Al, Be, Cu, Fe, Mg, Ni, Ti [1–13]; most of these are focusing on results from tools with a die angle equal to 90°.

In this work the texture of Cu during ECAP-deformation with a 120° die angle tool by route A and C has been determined by two methods: X-ray diffraction (standard, macro-level) and electron back scatter patterning (EBSD) (meso/micro--level). The characteristics of the texture due to route as well as the differences to a 90° die angle are discussed in [14]. The investigation focused on the comparison of the resulting textures with special respect to the deformation induced fragmentation. This is very interesting as the two methods determine textures on a very different size level. The imaging by the EBSP method allows also for consideration of the microstructural evolution.

2. Experiment

The die for ECAP used in present work had a square cross section with dimensions of 15×15 mm^2 and a die angle equal to 120°. For processing, copper samples were machined with dimensions of $35 \times 15 \times 15$ mm and annealed at 650 ℃ for 2 hours. Due to this treatment the material exhibited a strong cube texture due to recrystallisation.

For the case of route C the samples have been rotated by 180° around the axis number 1 between successive passes. For the standard texture measurements the samples were cut using a wire machine in the centre of the sample at a plane containing directions 1 and 2. From the cut surfaces, about 2 mm of the sample have been removed by grinding, then they were mechanically polished and finally etched. The textures were taken from surfaces containing directions 1 and 2 (Fig. 1), by X-ray CuK_α radiation, from the diffraction planes {111}, {200} {220}, and {311}. After having corrected the raw, incomplete pole figure data for defocusation and background, orientation distribution functions (ODF) have been calculated with the usage of LABOSOFT "LaboTex" software.

In the case of the EBSD investigations the samples additionally were electropolished. The same sample sites have been investigated using a LEICA Stereoscan 440, whereas the investigated sample area was considerably smaller than by the X-ray diffraction measurements. The evaluation of the ODF was performed with orientation imaging microscopy (OIM) software.

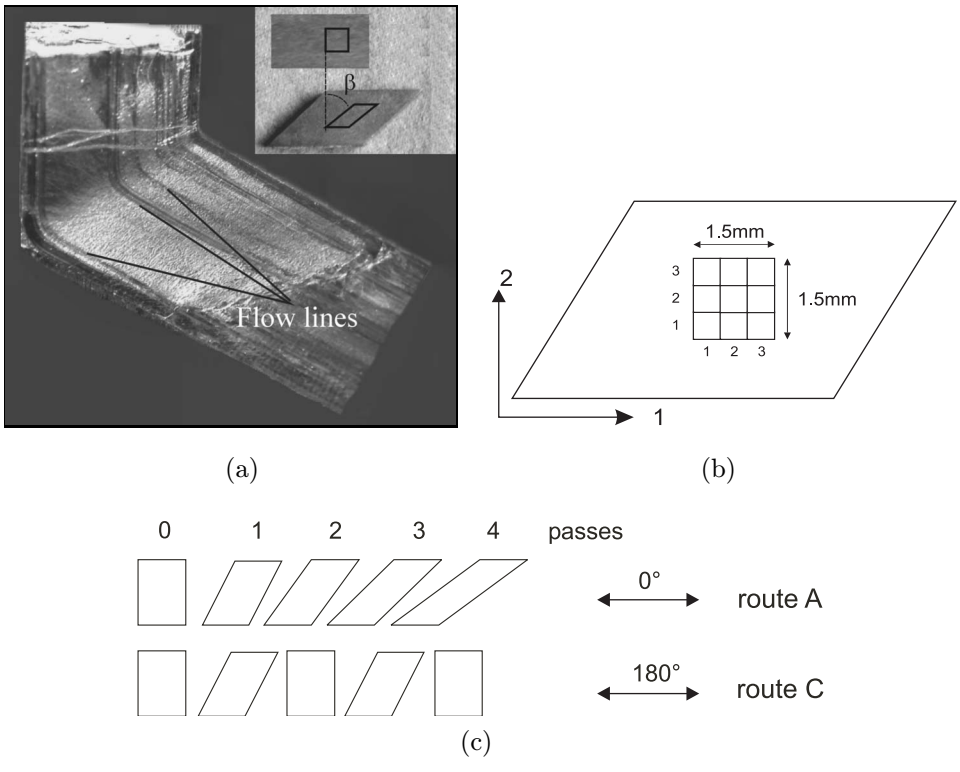

Fig. 1. Geometry of the macroscopic deformation (a); scan geometry of EBSD-scan after one pass (b); sample geometry after route A and C deformation up to 4 passes (c).

All ODFs are presented in Euler-space (Bunge's notation) as a function of the three Euler angles (ϕ_1, Φ, ϕ_2). Considering the large number of investigated samples, only the $\phi_2 = 0°$ and 45° sections are shown.

3. Results

In Figs. 2a and 2b the orientation maps are shown after one ECA pass and of the undeformed specimen, respectively. In all maps the colour designates the orientation with respect to the surface normal direction according to the colour key of the unit triangle (Fig. 2c). All patterns were subjected to a cleaning procedure in order to remove points of the frame, which cannot be evaluated by the OIM system software. The whole pattern corresponds to an area of 1500 × 1500 μm^2 on the sample and consists of 9 single scans of 500 × 500 μm^2 which have been measured with overlaps and then were fitted to each other. The directions 1 and 2 are indicated corresponding to Fig. 1.

Figure 3 shows the EBSD scans for the two different routes A and C for 2, 3 and 4 passes. The scans are all of 500 μm in width and 250 μm in height, except the

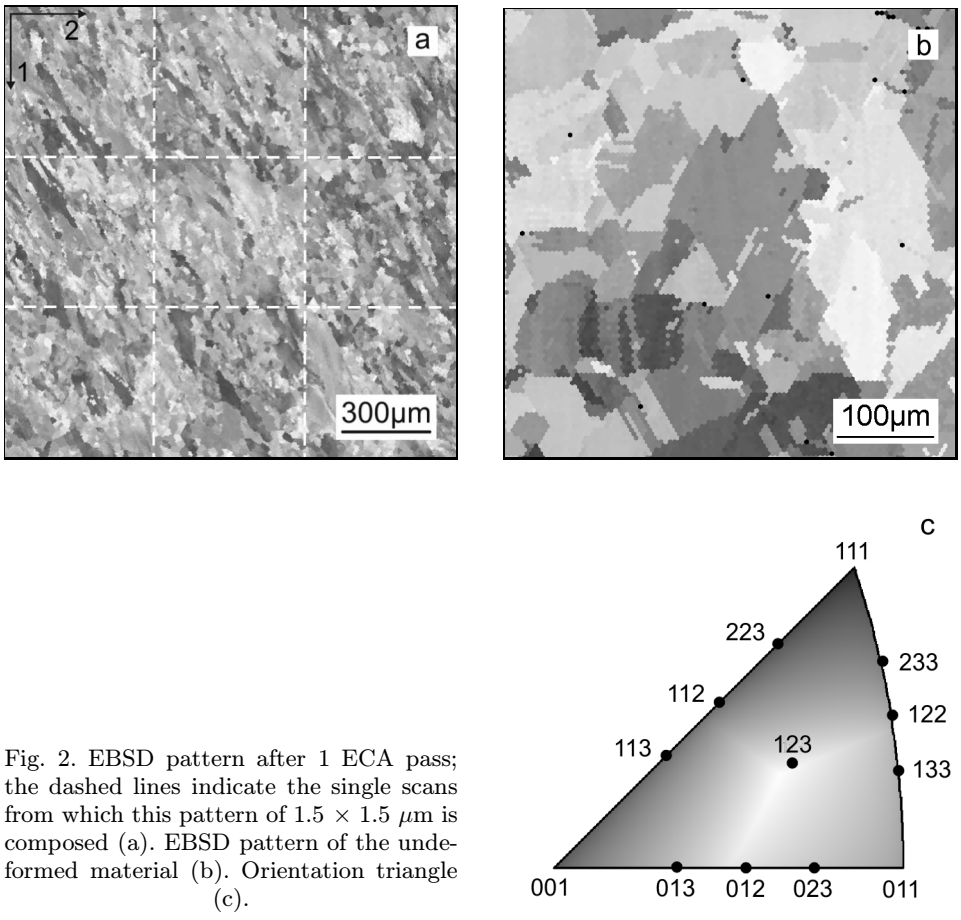

Fig. 2. EBSD pattern after 1 ECA pass; the dashed lines indicate the single scans from which this pattern of 1.5 × 1.5 μm is composed (a). EBSD pattern of the undeformed material (b). Orientation triangle (c).

scan after 4 passes route A (125 μm in height). The difference in the microstructure of the 2 different deformation regimes can be seen very clearly: a lamellar shape of grains after route A, corresponding to the repeating shear deformation with the same direction (left); and a grain shape similar to the initial structure related to the alternating shear direction because of the sample rotation performed with route C (right).

From the information of the complete orientation data of the EBSD scan of Fig. 2, the orientation distribution function can be evaluated from a single scan (Fig. 4a) and from the complete scan (Fig. 4b). The orientation distribution function resulting from the standard X-ray texture measurements is directly placed beside in Fig. 4c. It can easily be seen that there is no good correlation between the ODFs determined from the small sample area and that evaluated from the standard texture measurement.

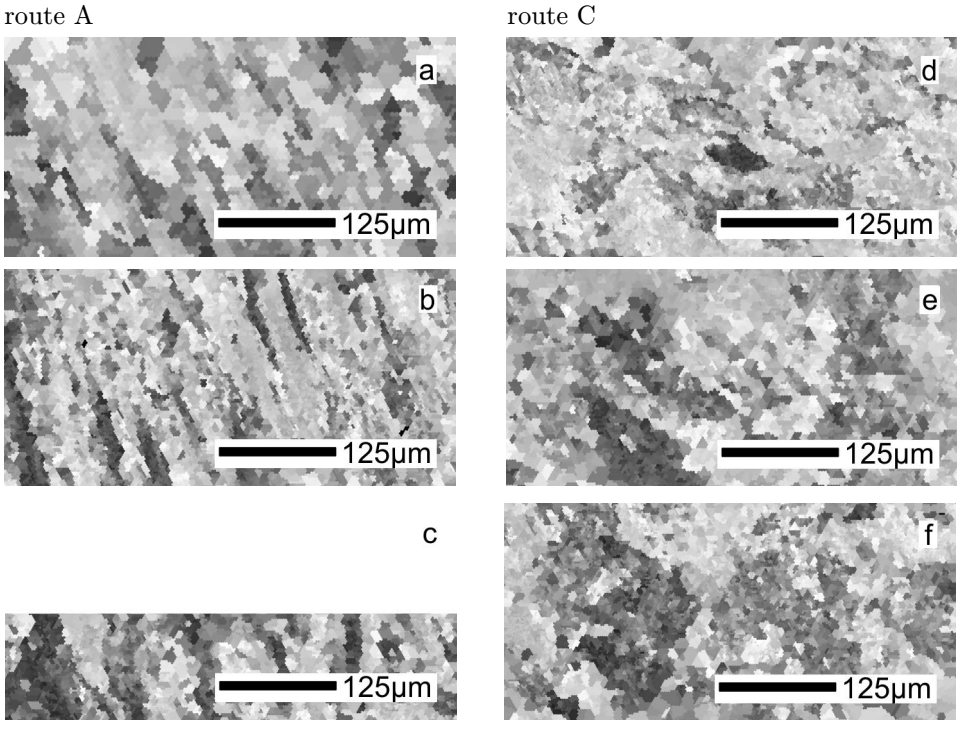

Fig. 3. EBSD patterns after 2 passes (a), 3 passes (b) and 4 passes (c) of ECA-route A and after 2 passes (d), 3 passes (e) and 4 passes (f) of ECA-route C, respectively.

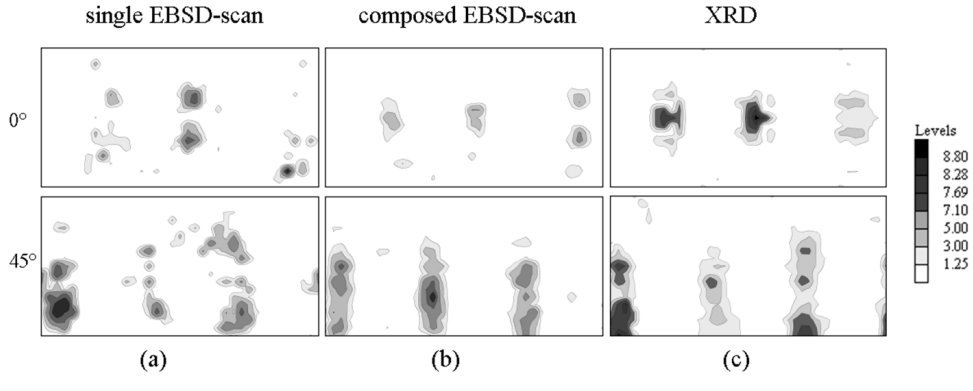

Fig. 4. Cuts of constant ϕ_2 (0° and 45°) of the orientation distribution function after 1 ECA-pass: determined by EBSD from one typical single scan (a) and from the complete composed scan (b); evaluated from the standard X-ray texture measurement (c) ($0 \leq \phi_1 \leq 180$ – horizontal, $0 \leq \Phi \leq 90$ – vertical).

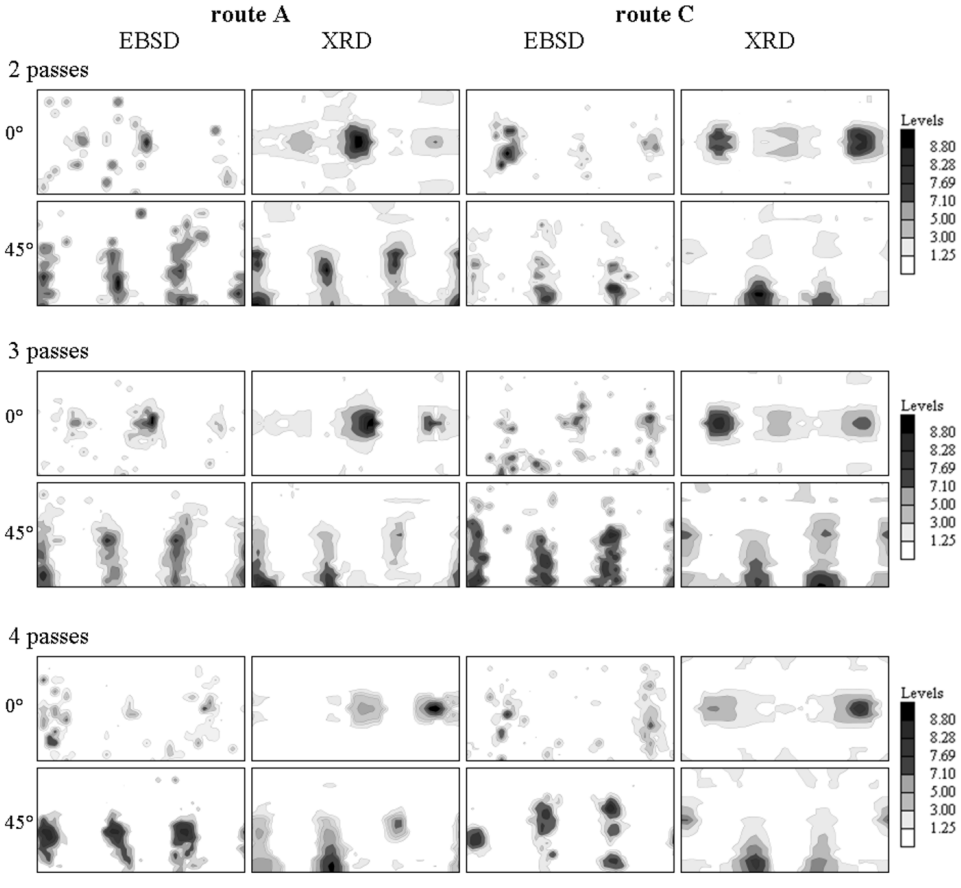

Fig. 5. Cuts of constant ϕ_2 (0° and 45°) of the orientation distribution functions as determined by EBSD and XRD for 2, 3 and 4 passes of ECA-routes A and C, respectively ($0 \leq \phi_1 \leq 180$ – horizontal, $0 \leq \Phi \leq 90$ – vertical).

In the following the ODFs determined from EBSD measurements and standard X-ray texture measurements, respectively, for 2, 3 and 4 passes of route A and C are presented side by side in Fig. 5. Very good accordance between micro- and macrotexture is observable for both routes even the EBSD-ODFs were obtained from scans of 500 × 250 μm^2 in size.

4. Discussion

In early discussions of the strain path during ECA pressing it was assumed that it could be simplified to simple shear on a plane bisecting the die angle [3, 4].

More recent work has analysed the strain history of a volume element following the flow "lines" (better flow "bands") through the die [15, 16, 17]. This model has been used successfully to describe even details of the deformation texture [15, 17, 18]. The macroscopic observation of flow lines in Fig. 1 and the change of the specimen shape seems to indicate that the integral strain can be simplified as shear parallel to the flow bands as proposed by Toth et al. [15, 16, 17].

4.1 Microstructure

Going to the microstructural level in Fig. 2 the EBSD pattern of a sample after one single ECA pass shows elongated grain/subgrain shapes, which are oriented in correspondence to the macroscopic shape change. With increasing pass number there has to be distinguished between Route A and C deformation. In the left part of Fig. 3 the EBSD patterns after 2 passes (a), 3 passes (b) and 4 passes (c) of route A deformation is shown. The orientation of the elongated grains indicates the successive shear with each pass. Also the increasing fragmentation is apparent as the subdivision of the grains results in small differences of the colour. The deformation in route C exhibits a completely different microstructure (Fig. 3d–f), as the shape of the original grains is more equiaxed and resembles to the microstructure of the undeformed material even after 4 passes. This can be attributed to the opposite direction of the shear deformation when rotating the sample for 180° after each pass. However, as a consequence of the high imposed strains the deformation induced defects lead also here to further fragmentation of the material, resulting in the improved mechanical properties like high strength and enhanced ductility of materials after severe plastic deformation (SPD) [19].

4.2 Texture

Generally the texture developing with each deformation pass using a 120° tool in the current investigation is not so strong compared to ECAP deformation using a 90° tool [15]. This corresponds to the lower amount of deformation per pass. The effective shear strain $\gamma = 0.85$ for one pass of the 120° tool has been obtained from the inset in Fig. 1a, the shear strain of the 90° tool was determined by the combination of the measurement and the simulation of the texture by the viscoplastic Taylor model and amounts to $\gamma = 2$ for one pass [15]. A quantitative analysis of the orientation distribution revealed three dominating texture components developing quite rapidly after the first ECAP pass: $\{111\}\ \langle 011\rangle$, $\{112\}\ \langle 011\rangle$ and $\{110\}\ \langle 112>$ (*Brass*) (in the order of magnitude). The development of the $\{111\}\ \langle 011\rangle$- and the $\{112\}\ \langle 011\rangle$-component is reasonable since they are ideal shear components, the brass-component usually occurs in the texture of rolled materials. Right after the first ECAP pass the initial strong cube-texture of the annealed state is strongly reduced to a fraction smaller than those of the mentioned components.

In Figs. 4a and 4c the comparison of the orientation distribution functions obtained from a single EBSD-scan of 500 × 500 μm^2 size (a) and determined by the standard X-ray diffraction technique (c) shows no good correspondence. This is also found when considering the other 8 single scans. That is quite plausible as the illuminated area on the sample is about 2 mm^2, whereas one single EBSD scan only amounts to 0.25 mm^2. After putting together the patchwork the resulting orientation distribution function (Fig. 4b) naturally agrees very well with the ODF determined by XRD. The reason is the size relation between the investigated area and the grains. The initial grain size of the material is about 100 μm, after one ECA pass the deformation leads to subgrain-like misorientations inside the grains, but the fragmentation in the sense of high angle boundaries cannot be expected to be very progressed. So the smaller EBSD scan area cannot provide the statistics necessary for obtaining a global orientation distribution as it is done by the XRD method. After increasing the area (= statistics) by a factor of 9 by considering more scans the investigated volume of the two methods is comparable.

At higher deformations this situation changes to the better. After two ECA--passes, irrespective of route type, more same texture components arise from a small EBSD-scan of 500 × 250 μm^2 as well as measured by X-ray diffraction, however, the intensities are quite different. This is obviously related to the fact that the additional deformation makes the texture stronger and more uniform throughout the material. But what is the microstructural background of this change? Certainly it must be related with the progressing fragmentation of the material with increasing deformation. More precisely, the refinement as well as the increasing misorientation between the grains/subgrains has increased enough, so that the statistical criterion to obtain full orientation information is also fulfilled investigating only smaller areas. In Fig. 5 it can be seen that the characteristics of the orientation distributions determined by EBSD are quite akin to those ODFs evaluated from the X-ray diffraction data.

These experimental results of the texture evolution support the recent "flow--line" model simulations [15, 16, 17] definitely for the case of route A.

5. Summary

The microstructural evolution after ECA pressing in the two routes A and C exhibits basic differences as well as similarities. The alternating shear direction when processing route C results in roughly equiaxed grains, while each pass of route A leads to a further elongation and rotation of the grains with respect of the macroscopic sample directions. As a common feature the high imposed strains cause formation of new boundaries subdividing the old grains. With proceeding deformation the increasing misorientation in this subgrain structure leads to further fragmentation of the material. This accounts for the good correspondence between

microtexture determined by EBSD on relatively small areas and macrotexture obtained by XRD at elevated strains.

When texture is determined by EBSP care must be taken to make the scanned volume large enough. If the number of contributing grains is too small the local statistical fluctuations may mislead to the impression of an inhomogeneous texture. True heterogeneities of texture – if any – should be considered on a scale comparable to the dimensions of the workpiece (e.g., surface textures on rolled sheets [20]).

The resulting experimental textures verify the of texture evolution as simulated using recent flow line model.

Acknowledgements

The Science Foundation of Austria (FWF) is acknowledged for financial support under projects P17095-N01 and P17095-N02.

REFERENCES

[1] VOGEL, S. C.—BEYERLEIN, I. J.—BOURKE, M. A. M.—TOMÉ, C. N.—RANGASWAMY, P.—XU, C.—LANGDON, T. G.: Mater. Sci. Forum, *408−412*, 2002, p. 73.

[2] FIELD, R. D.—HARTWIG, K. T.—NECKER, C. T.—BINGERT, J. F.—AGNEW, S. R.: Metal. Mater. Trans. A, *33A*, 2002, p. 965.

[3] AGNEW, S. R.—KOCKS, U. F.—HARTWIG, K. T.—WEERTMAN, J. R.: In: Proc. 19th Riso Int. Symp. Mater. Sci. Eds.: Carstensen J. V. et al. Roskilde, DK, Riso Nat. Lab. 1998, p. 201.

[4] AGNEW, S. R.: In: Proc. 12th Conf. on Textures of Materials. Ed.: Szpunar, J. A. Ottawa, NRC Research Press 1999, p. 575.

[5] KUSNIERZ, J.: Mater. Sci. Forum, *426–432*, 2003, p. 2807.

[6] VOGEL, S. C.—ALEXANDER, D. J.—BEYERLEIN, I. J.—BOURKE, M. A. M.—BROWN, D. W.—CLAUSEN, B.—TOMÉ, C. N.—VON DREELE, R. B.—XU, C.—LANGDON, T. G.: Mater. Sci. Forum, *426–432*, 2003, p. 2661.

[7] GIBBS, M. A.—HARTWIG, K. T.—CORNWELL, L. R.—GOFORTH, R. E.—PAYZANT, E. A.: Scripta Mater., *39*, 1998, p. 1699.

[8] KIM , W. J.—HONG, S. I.—KIM, Y. S.—MIN, S. H.—JEONG, H. T.—LEE, J. D.: Acta Mater., *51*, 2003, p. 3293.

[9] AGNEW, S. R.—HORTON, J. A.—LILLO, T. M.—BROWN, D. W.: Scripta Mater., *50*, 2004, p. 377.

[10] STOICA, G. M.—AGNEW, S. R.—PAYZAN, E. A.—CARPENTER, D. A.—CHEN, L. J.—LIAW, P. K.: In: TMS Proc. Ultrafine Grained Materials 3 Symposium. Eds.: Zhu, Y. T., Langdon, T. G., Valiev, R. Z., Semiatin, S. L., Shin, D. H., Lowe, T. C. Warrendale, TMS publications 2004, p. 427.

[11] SKROTZKI, W.—TAMM, R.—KLEMM, R.—THIELE, E.—HOLSTE, C.—BAUM, H.: Mater. Sci. Forum, *408–412*, 2002, p. 667.

[12] YU, S. H.—SHIN, D. H.—PARK, N. J.—HUH, M. Y.—HWANG, S. K.: Mater. Sci. Forum, *408–412*, 2002, p. 661.

[13] YU, S. H.—SHIN, D. H.—HWANG, S. K.: In: TMS Proc. Ultrafine Grained Materials 3 Symposium. Eds.: Zhu, Y. T., Langdon, T. G., Valiev, R. Z., Semiatin, S. L., Shin, D. H., Lowe, T. C. Warrendale, TMS publications 2004, p. 227.

[14] SCHAFLER, E.—TARKOWSKI, L.—BONARSKI, J.—KOPACZ, I.—PIPPAN, R.—STÜWE, H. P.: Arch. Metall., *53*, 2005, p. 436.
[15] TÓTH, L. S.—KOPACZ, I.—ZEHETBAUER, M.—ALEXANDROV, I.: In:. Proc. THERMEC 2000, Las Vegas. Eds.: Chandra, T., Higashi, K., Suryanarayana, C., Tome, C. CD-ROM. Special Issue of J. Mater. Processing Technol. 2001. London, Elsevier Science 2001.
[16] TÓTH, L. S.—ARRUFFAT MASSION, R.—GERMAIN, L.—BAIK, S. C.—SUWAS, S.: Acta Mater., *52*, 2004, p. 1885.
[17] TÓTH, L. S.: Adv. Eng. Mater., *5*, 2003, p. 308.
[18] KOPACZ, I.—ZEHETBAUER, M.—TÓTH, L. S.—ALEXANDROV, I. V.—ORTNER, B.: In: Proc. 22nd Riso Int. Symp. On Mech. Sci. Eds.: Dinesen, A. R. et al. Roskilde, DK, Riso Nat. Lab. 2001, p. 295.
[19] VALIEV, R. Z.—ISLAMGALIEV, R. K.—ALEXANDROV, I. V.: Progr. Mater. Sci., *45*, 2000, p. 103.
[20] REGENET, P. J.—STUEWE, H. P.: Z. Metallk., *54*, 1963, p. 273.